Volume-based Translation of phase-cycle balanced Steady State Free Precession MRI to Diffusion Tensor

Thesis submitted in partial fulfilment of the requirements for the degree

Master of Science

Graduate School of Neuroscience
Faculty of Science
Faculty of Medicine
University of Tübingen

Presented by
Fabian Klopfer, M.Sc.
from Villingen-Schwenningen, Germany

Tübingen, 2024

Thesis Advisor	Dr. Rahel Heule Department for High-field Magnetic Resonance Max Planck Institute for Biological Cybernetics Center for MR Research Children's Hospital University of Zurich
Second Advisor	Prof. Dr. Klaus Scheffler Department for High-field Magnetic Resonance Max Planck Institute for Biological Cybernetics

Disclosures

- I affirm that I have written the dissertation myself and have not used any sources and aids other than those indicated.
- I affirm that I have not included data generated in one of my laboratory rotations and already presented in the respective laboratory report.

Tübingen, March 2024 _____

Abstract:

Lorem ipsum dolor sit amet, consectetuer adipiscing elit. Ut purus elit, vestibulum ut, placerat ac, adipiscing vitae, felis. Curabitur dictum gravida mauris. Nam arcu libero, nonummy eget, consectetuer id, vulputate a, magna. Donec vehicula augue eu neque. Pellentesque habitant morbi tristique senectus et netus et malesuada fames ac turpis egestas. Mauris ut leo. Cras viverra metus rhoncus sem. Nulla et lectus vestibulum urna fringilla ultrices. Phasellus eu tellus sit amet tortor gravida placerat. Integer sapien est, iaculis in, pretium quis, viverra ac, nunc. Praesent eget sem vel leo ultrices bibendum. Aenean faucibus. Morbi dolor nulla, malesuada eu, pulvinar at, mollis ac, nulla. Curabitur auctor semper nulla. Donec varius orci eget risus. Duis nibh mi, congue eu, accumsan eleifend, sagittis quis, diam. Duis eget orci sit amet orci dignissim rutrum.

Contents

1. Introduction

- Largest multi modal data set of its kind
- bSSFP now feasible with new HW
- Speeds up scanning times potentially yielding multiple modalities with one scan
- Limited data available for ML applications

2. Background & Related Work

In this chapter, relevant background knowledge and related previously published work is discussed.

2.1. Magnetic Resonance Imaging

2.1.1. Fundamentals of MRI

MRI uses the ability of certrain nuclei to absorb and emit energy in the radio frequency spectrum to generate images of organisms. This ability is called Nuclear Magnetic Resonance and depends on charge, spin, and mass, which are the intrinsic properties of particles.
Nuclear Magnetic Resonance-active Nuclei are those atoms with with an odd number of protons and/or neurtons[26, 16]. They have a spin angular momentum defined as

$$S = \hbar I,$$

where I is the spin operator and $\hbar$ is Planck's constant normalized by 2π. The odd number of protons/neutrons also induces a magnetic dipole moment

$$\mu = \gamma S.$$

γ [MHz/T] is called the gyromagnetic ratio and is unique to each nuclear magnetic resonance-active nuclei. It is the ratio of the magnetic dipole moment μ to the spin of a particle S. The gyromagnetic ratio governs the frequency of precession and is meassured empirically.
Specifically, ^{1}H has a spin of 0.5, a high natural abundance of 0.998 and is therefore used primarily for clinical and medical MRI. its gyromagnetic ratio is $\gamma = 42.57$ MHz/T.
When placing such nucleie into a magnetic field, the spins have a tendency to align with its direction, leading to a net or bulk magnetization per unit volume (or voxel) v,

$$M = \sum_{v \in V} \mu_v.$$

Additionally, due to spin and mass, the nucleus exhibits an angular momentum, i.e. it precesses e.g. in a gravitational field. The dynamics of this angular momentum or pecession can be described by

$$\frac{d\mu}{dt} = \mu \times \gamma B,$$

when considering a single nucleus and for a summing over a unit volume

$$\frac{dM}{dt} = M \times \gamma B.$$

The combination of magnetic and angular momentum causes the nucleus to precess in a magnetic field as well with a specific frequency — called the Larmor frequency:

$$\omega = \gamma B,$$

where B $[T]$ is the strength of a magnetic field and γ is the gyromagnetic ratio.

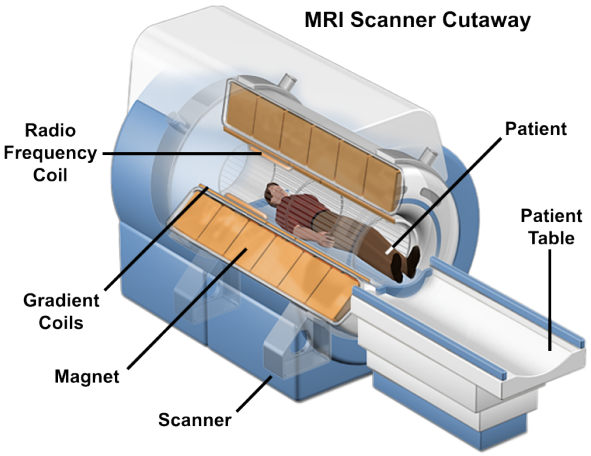

Figure 2.1. *MRI scanner with a part cut-away such that the main components are visible.*

A scanner MR scanner consists of a primary electromagnetic coil, that is surrounded by a cryostat and thermal insulation, an excitation coil, spatial localization coils, and a receiver coil, as shown in **??**. The excitation and the receiving coil are merged into one RF coil here.

This **primary electromagnet** provides the main magnetic field B_0 to polarize the NMR-active nuclei with field strengths up to $14.2T$, but usually about $1.5T$ to $3T$ in medical applications. This is several orders of magnitude larger than the earth magnetic field which is approximately 0.5 Gauss To provide such high fields, super-conductivity needs to be reached, thus the coil is cooled using liquid helium. The B_0 field is spatially uniform and temporally stable in an ideal scanner, such that the same polarization is applied to all atoms. In practice this field is not perfectly homogeneous, such that magnetic field probes are used to measure the field and shim cards are used to correct these inhomogenieties. This is called passive shimming. Alternatively, active shimming coils can be used to smooth the inhomogenieties. It is oriented along the "long" part of the scanner, so if a human lies in the scanner, the poles are oriented towards the head and the feet of the subject. We call this axis the z-axis.

Additionally, an **excitation system** is necessary to generate exciting magnetic pulses $B_1(t)$ to cause nutation of the nuclei of interest as well as to refocussing, spoiling, inversion and saturation. The $B_1(t)$ field is a radio frequency field with the excitation frequency defined by the B_0 field strength, the Larmor frequency of the excitation target nuclei and are both short in duration and amplitude. For example with $B_0 = 3\text{T}$ we get

$$42.58\frac{\text{MHz}}{\text{T}} \cdot 3\text{T} = 127.74\text{MHz}.$$

Typical pulse durations are on the intervall $[0.1, 10]$ ms and amplitude about $< 25\mu\text{T}$. The shape of the excitation pulse is governed by an envelope function in terms of amplitude trajectory. The excitation pulses are perpendicular to the B_0 field, which is important to enable the excitation pulses to tip the spin system in the presence of the strong polarizing field. While the B_0 field causes polarization, thus alignment and precession, the $B_1(t)$ pulses cause a "tipping" or nutation of the precession — shown in **??**, generating transverse magnetization such that it is detectable using Faraday's law of induction. An example of an excitation pulse is

$$B_1(t) = B_1(t)^e(t)\left(\cos\left(\omega_{RF}t + \theta\right)i - \sin\left(\omega_{RF}t + \theta\right)j\right),$$

with $B_1(t)^e(t)$ a pulse envelope function, e.g. `sinc` or `rect` functions, ω_{RF} the excitation carrier frequency which should match the Larmor frequency of the spin system, and $\hat{i}'$, $\hat{j}'$ the polarization directions. Additionally a RF pulse has a filp angle α which is the angle between the

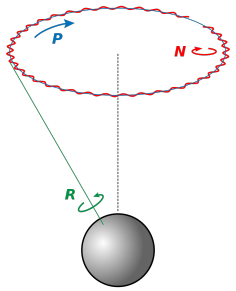

Figure 2.2. *A visualization of rotation r (in out case we call it spin) in green, precession p in blue — at the Larmor frequency — and nutation n in red.*

z-axis and the $B1$ pulse (called inclination in spherical coordinates) and a phase θ which is the angle in the xy plane, starting at the x-axis (azimuth in spherical coordinates). The excitation system is commonly implemented using a birdcage coil as it's highly efficient in terms of energy, excitation and heating mitigation. The $B_1(t)$ field is supposed to be highly uniform, especially radially while decaying slightly axially.

A **receiving coil(s)** reads out the response of the excited tissue. This can be the same RF coil that is used for excitation. As the precessing magnetization causes induction in the receiving coil(s), the flux in the receiving coil changes causing an electromotive force

$$\epsilon = -\frac{\partial \Phi}{\partial t}.$$

The picked up signal is further split up, multiplied by $\cos \omega_0 t$ and $\sin \omega_0 t$ respectively and low-pass filtered to get the in-phase signal $I(t)$ and the quadrature signal $Q(t)$. The These signals are then quantized, yielding $I(t)$ as the real and $Q(t)$ as the imaginary part of the signal.

The excitation forces the magnetization off from its equilibrium state and thus induces relaxation back to the equilibrium again after excitation. This relaxation can be separated into two components: longitudinal and transverse relaxation.

The longitudinal component can be described as a return to the equilibrium state of the magnetization on the z-axis

$$\frac{dM_z}{dt} = -\frac{M_z - M_e}{T_1},$$

where M_e is the equilibrium nuclear magnetization, which is proportional to the applied magnetic field B_0 [26]. The solution to this equation is

$$M_z = M_e + (M_z - M_e) \exp -t/T_1.$$

T_1 is the time constant of the longitudinal component also called longitudinal relaxation time constant or spin-lattice time constant. It is proportional to the applied field strength and thus lengthens when B_0 is increased in strength. Practically, it is the time that it takes for M_z to return to 63% of it's thermal eqilibrium state M_e [5, 23].

The transversal component can be formulated as a decay process

$$\frac{dM_{xy}}{dt} = -\frac{M_{xy}}{T_2}.$$

Accordingly, T_2 is the time constant of the transverse relaxation component, also called spin-spin relaxation time constant. It is mostly independent from the B_0 field strength and $T_2 \leq T_1$. T_2 is more rapid, the less mobile the spins are, i.e. T_2 is larger in water than in solids. Practically, in one T_2, M_{xy} loses 63% of it's magnetization right after excitation.

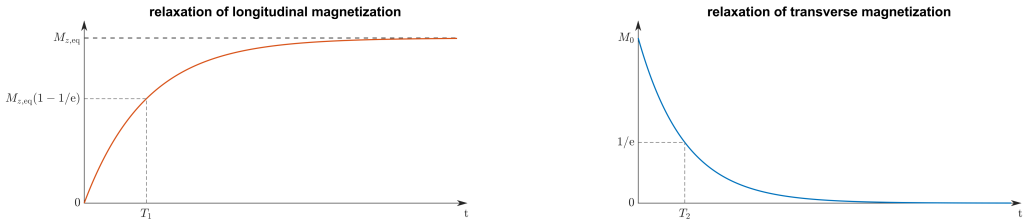

Figure 2.3. ***Left:*** *T_1 relaxation curve shows the return to the equilibrium state.* ***Right:*** *T_2 relaxation curve visualizes the transveral magnetization decay to zero.*

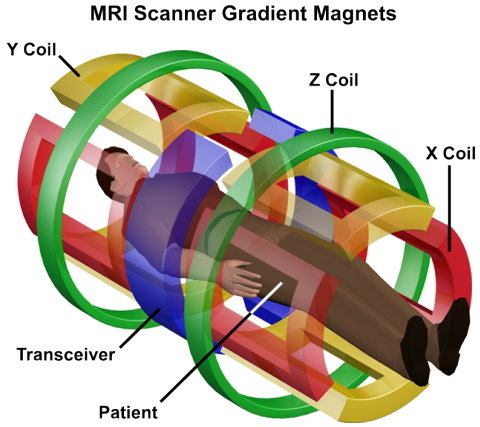

Figure 2.4. *A conceptual visualization of the gradient coils of an MRI scanner.*

A **Gradient system** are used to select regions of interest from the full organism and to iterate over different regions.

In order to describe the bSSFP sequence later on, the notions of **the lab and the rotating frame** will be introduced now. The laboratory frame is the frame of reference from the view in which the room or the scanner is anchored. The coordinate system is defined based on the B_0 field, where the z-axis is in the direction of the B_0 field, i.e. from the feet of the subject in the scanner to its head. The x-axis is parallel to the floor, while the y-axis is parallel to the walls. Put differently, y corresponds to the height, x to the width and z to the depth of the room. In this frame, we can observe rotation/spin, precession and rotation. In contrast, the rotating frame, the rotational/spinning and the precessional behavior is factored out, such that only the nutational information is preserved. This can be achieved with a transformation of the xy-plane, while the z-axis stays the same as in the lab frame. Intuitively, the xy plane in the rotational frame is rotating at frequency ω relative to the xy-axis of the lab frame.

The equation of motion for a system of spins in the lab frame can be described by the Bloch equation, which consists of the precession & nutation, the transversal and the longitudinal relaxation terms:

$$\frac{dM}{dt} = M \times \gamma B - \frac{M_x i + M_y j}{T_2} - \frac{(M_z - M_e)k}{T_1}.$$

B aggregates the static B_0 field, the excitation $B_1(t)$ field and the gradient $G(t)$ fields.

Let $M_R = \left(M_{x'}, M_{y'}, M_z\right)^T$, $B_R = \left(B_{x'}, B_{y'}, B_z\right)$, R_z the rotation matrix around the z-axis, $M = R_z(\omega t)M_R$ and $B = R_z(\omega t)B_R$. When defining the tranverse magnetization as complex $M_R(t) = M_{x'}(t) + M_{y'}(t)$ for the rotating frame and $M(t) = M_x(t) + iM_y(t)$ we can relate the lab and the rotating frame via

$$M(t) = M_R(t) \exp -i\omega t$$

and with ω the Larmor frequency, $M_{x'}$ and $M_{y'}$ become constants without excitation pulses. With this we can reformulate the Bloch equation in the rotating frame

$$\frac{dM}{dt} = M_R \times \gamma B_{\text{eff}} - \frac{M_{x'}i + M_{y'}j}{T_2} - \frac{(M_z - M_e)k}{T_1},$$

where

$$B_{\text{eff}} = \frac{\omega_R}{\gamma} + B_R$$

and $\omega_R = (0, 0, -\omega)$.

Finally, Computers control the different coils, store the meassurements and reconstruct images from the meassured magnetizations.

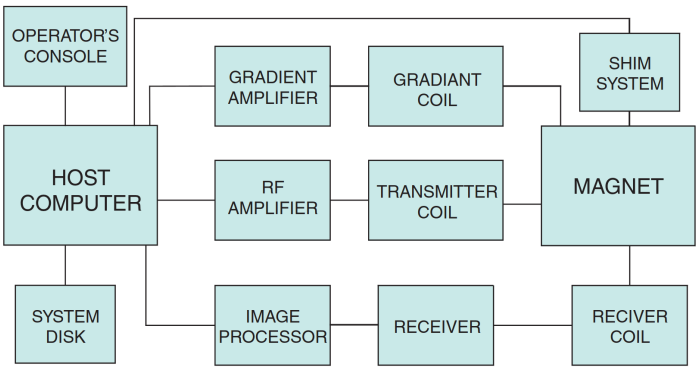

Figure 2.5. *Block diagram of the components in an MRI scanner system*

Excitation Sequences

2.1.2. balanced Steady-State Free Precession Imaging

In depth description of sequence, profile, banding

2.1.3. Diffusion-weighted Imaging

2.2. Deep Learning

2.2.1. Fundamentals of Neuronal Networks

2.2.2. Architecture & Training

UNet, challenges, impact of transformers, ...

2.2.3. Image-to-Image Synthesis

2.2.4. Deep Learning in Medical Imaging

3. Methods

3.1. The Dove Dataset

Some stats on size

3.1.1. Participants & Study Design

briefly describe participants, task, scanning times (of the day)

3.1.2. Recorded Sequences

cf gais doc. Details on acquisitions

3.2. Data Processing

requirements

3.2.1. bSSFP

3.2.2. DWI

TODO ask svenja what was done

3.2.3. Augmentation

3.3. Machine Learning-based DWI Tensor estimation from bSSFP data

MONAI, torchio, pytorch lightning.

3.3.1. Architecture

UNet + some extra layers to fit output dim.

3.3.2. Training

Pre-training, transfer & fine-tuning

Sparse data, small batch sizes. => Augmentation not enough => Pre training

AutoEncoder PreTraining As auto encoder. train autoenc for bssfp only

ExtraHead Transfer and Fine tuning freeze autoenc, add head. transfer then unfreeze all and fine tune Unet + extra head

4. Results

4.1. Direct bSSFP to DWI Tensor Training

4.2. Pre-Training & bSSFP Transfer-Learning

4.3. Comparison of Voxel-wise to Volume-wise Regression

4.4. Modality Comparisons

4.4.1. Quantitative comparison of Quality differences between Auto-Encoding and pc-bSSFP Image to Image Translation

4.4.2. pc-bSSFP is more suitable than single-volume Structural Images

4.4.3. Phase-cycles contain relevant the Information

4.4.4. Asymmetry Index Maps distill phase-cycle Information

5. Discussion

5.1. Limitations

voxel- patch - volume pro-con
Statistical power
model size/speed
learned vs. closed-form/deduced/analytical transformation

5.2. Future Work

5.2.1. Modular Deep Learning

Pretrain autoenc for both.
Use enc of bssfp (or conv transf. for enc) and dec of DWI/specialized for modality
LDM for latent translation
GAN & Stable diffusion, control flow matching, latent diffusion models

5.2.2. Conv Transf.

New kid on the block

5.2.3. Neural Arch Search

DiNTS

6. Acknowledgements

Rahel, Flo, Qi, Klaus

Bibliography

[1] Matt A. Bernstein, Kevin F. King, and Xiaohong Joe Zhou. *Handbook of MRI Pulse Sequences*. en. Google-Books-ID: d6PLHcyejEIC. Elsevier, Sept. 2004. ISBN: 978-0-08-053312-4.

[2] Oliver Bieri and Klaus Scheffler. "Fundamentals of balanced steady state free precession MRI". en. In: *Journal of Magnetic Resonance Imaging* 38.1 (2013). _eprint: https://onlinelibrary.wiley.com pp. 2–11. ISSN: 1522-2586. DOI: 10.1002/jmri.24163. URL: https://onlinelibrary.wiley.com/doi/abs/10.1002/jmri.24163 (visited on 04/10/2024).

[3] Florian Birk et al. "High-resolution neural network-driven mapping of multiple diffusion metrics leveraging asymmetries in the balanced steady-state free precession frequency profile". en. In: *NMR in Biomedicine* 35.6 (2022). _eprint: https://onlinelibrary.wiley.com/doi/pdf/10.1002/n e4669. ISSN: 1099-1492. DOI: 10.1002/nbm.4669. URL: https://onlinelibrary.wiley.com/doi/abs/10.1002/nbm.4669 (visited on 04/11/2024).

[4] Stevo Bozinovski. "Reminder of the First Paper on Transfer Learning in Neural Networks, 1976". en. In: *Informatica* 44.3 (Sept. 2020). Number: 3. ISSN: 1854-3871. DOI: 10.31449/inf.v44i3.2828. URL: https://www.informatica.si/index.php/informatica/article/view/2828 (visited on 04/10/2024).

[5] Brian M. Dale, Mark A. Brown, and PhD„ Richard C. Semelka. "Relaxation". en. In: *MRI Basic Principles and Applications*. Section: 3 _eprint: https://onlinelibrary.wiley.com/doi/pdf/10.1002/97 John Wiley & Sons, Ltd, 2015, pp. 17–25. ISBN: 978-1-119-01306-8. DOI: 10.1002/9781119013068.ch3. URL: https://onlinelibrary.wiley.com/doi/abs/10.1002/9781119013068.ch3 (visited on 04/18/2024).

[6] M. Jorge Cardoso et al. *MONAI: An open-source framework for deep learning in healthcare*. arXiv:2211.02701 [cs]. Nov. 2022. DOI: 10.48550/arXiv.2211.02701. URL: http://arxiv.org/abs/2211.02701 (visited on 04/10/2024).

[7] Sihong Chen, Kai Ma, and Yefeng Zheng. *Med3D: Transfer Learning for 3D Medical Image Analysis*. arXiv:1904.00625 [cs]. July 2019. DOI: 10.48550/arXiv.1904.00625. URL: http://arxiv.org/abs/1904.00625 (visited on 04/10/2024).

[8] Alexandra Chronopoulou, Christos Baziotis, and Alexandros Potamianos. "An Embarrassingly Simple Approach for Transfer Learning from Pretrained Language Models". In: *Proceedings of the 2019 Conference of the North American Chapter of the Association for Computational Linguistics: Human Language Technologies, Volume 1 (Long and Short Papers)*. Ed. by Jill Burstein, Christy Doran, and Thamar Solorio. Minneapolis, Minnesota: Association for Computational Linguistics, June 2019, pp. 2089–2095. DOI: 10.18653/v1/N19-1213. URL: https://aclanthology.org/N19-1213 (visited on 04/10/2024).

[9] Dan Dale. *Fine-Tuning Scheduler*. Mar. 2024. DOI: 10.5281/zenodo.10780386. URL: https://zenodo.org/records/10780386 (visited on 04/10/2024).

[10] Thijs Dhollander. "From Diffusion to the Diffusion Tensor". en. In: *Diffusion Tensor Imaging: A Practical Handbook*. Ed. by Wim Van Hecke, Louise Emsell, and Stefan Sunaert. New York, NY: Springer, 2016, pp. 37–63. ISBN: 978-1-4939-3118-7. DOI: 10.1007/978-1-4939-3118-7_4. URL: https://doi.org/10.1007/978-1-4939-3118-7_4 (visited on 04/10/2024).

[11] William A. Falcon. “Pytorch lightning”. In: *GitHub* 3 (2019). URL: https://cir.nii.ac.jp/crid/1370013168774120069 (visited on 04/10/2024).

[12] K. J. Friston et al. “Statistical parametric maps in functional imaging: A general linear approach”. en. In: *Human Brain Mapping* 2.4 (1994). _eprint: https://onlinelibrary.wiley.com/doi/pdf/10.10 pp. 189–210. ISSN: 1097-0193. DOI: 10.1002/hbm.460020402. URL: https://onlinelibrary.wiley.com/doi/abs/10.1002/hbm.460020402 (visited on 04/10/2024).

[13] Eleftherios Garyfallidis et al. “Dipy, a library for the analysis of diffusion MRI data”. English. In: *Frontiers in Neuroinformatics* 8 (Feb. 2014). Publisher: Frontiers. ISSN: 1662-5196. DOI: 10.3389/fninf.2014.00008. URL: https://www.frontiersin.org/articles/10.3389/fninf.2014.00008 (visited on 04/10/2024).

[14] Ian Goodfellow, Yoshua Bengio, and Aaron Courville. *Deep Learning*. en. Google-Books-ID: omivDQAAQBAJ. MIT Press, Nov. 2016. ISBN: 978-0-262-33737-3.

[15] Timofey Grigoryev, Andrey Voynov, and Artem Babenko. “When, Why, and Which Pretrained GANs Are Useful?” en. In: Oct. 2021. URL: https://openreview.net/forum?id=4Ycr8oeCoIh (visited on 04/10/2024).

[16] David Halliday, Robert Resnick, and Jearl Walker. *Fundamentals of Physics*. en. Google-Books-ID: HybkAwAAQBAJ. John Wiley & Sons, Aug. 2013. ISBN: 978-1-118-23071-8.

[17] Rahel Heule, Carl Ganter, and Oliver Bieri. “Triple echo steady-state (TESS) relaxometry”. en. In: *Magnetic Resonance in Medicine* 71.1 (2014). _eprint: https://onlinelibrary.wiley.com/doi/pd pp. 230–237. ISSN: 1522-2594. DOI: 10.1002/mrm.24659. URL: https://onlinelibrary.wiley.com/doi/abs/10.1002/mrm.24659 (visited on 04/10/2024).

[18] Jeremy Howard and Sebastian Ruder. “Universal Language Model Fine-tuning for Text Classification”. In: *Proceedings of the 56th Annual Meeting of the Association for Computational Linguistics (Volume 1: Long Papers)*. Ed. by Iryna Gurevych and Yusuke Miyao. Melbourne, Australia: Association for Computational Linguistics, July 2018, pp. 328–339. DOI: 10.18653/v1/P18-1031. URL: https://aclanthology.org/P18-1031 (visited on 04/10/2024).

[19] T.A.G.M. Huisman. “Diffusion-weighted and diffusion tensor imaging of the brain, made easy”. In: *Cancer Imaging* 10.1A (Oct. 2010), S163–S171. ISSN: 1740-5025. DOI: 10.1102/1470-7330.2010.9023. URL: https://www.ncbi.nlm.nih.gov/pmc/articles/PMC2967146/ (visited on 04/10/2024).

[20] Phillip Isola et al. “Image-To-Image Translation With Conditional Adversarial Networks”. In: 2017, pp. 1125–1134. URL: https://openaccess.thecvf.com/content_cvpr_2017/html/Isola_Image-To-Image_Translation_With_CVPR_2017_paper.html (visited on 04/10/2024).

[21] Pavel Izmailov et al. *Averaging Weights Leads to Wider Optima and Better Generalization*. arXiv:1803.05407 [cs, stat]. Feb. 2019. DOI: 10.48550/arXiv.1803.05407. URL: http://arxiv.org/abs/1803.05407 (visited on 04/10/2024).

[22] Yann LeCun, Yoshua Bengio, and Geoffrey Hinton. “Deep learning”. en. In: *Nature* 521.7553 (May 2015). Publisher: Nature Publishing Group, pp. 436–444. ISSN: 1476-4687. DOI: 10.1038/nature14539. URL: https://www.nature.com/articles/nature14539 (visited on 04/10/2024).

[23] Zhi-Pei Liang and Paul C. Lauterbur. *Principles of Magnetic Resonance Imaging*. SPIE Optical Engineering Press Bellingham, 2000. URL: https://cds.cern.ch/record/1480847/files/0780347234_TOC.pdf (visited on 04/17/2024).

[24] Ilya Loshchilov and Frank Hutter. *Decoupled Weight Decay Regularization*. arXiv:1711.05101 [cs, math]. Jan. 2019. DOI: 10.48550/arXiv.1711.05101. URL: http://arxiv.org/abs/1711.05101 (visited on 04/10/2024).

[25] Damien Nguyen and Oliver Bieri. "Motion-insensitive rapid configuration relaxometry". en. In: *Magnetic Resonance in Medicine* 78.2 (2017). _eprint: https://onlinelibrary.wiley.com/doi/pdf/10.1 pp. 518–526. ISSN: 1522-2594. DOI: 10.1002/mrm.26384. URL: https://onlinelibrary.wiley.com/doi/abs/10.1002/mrm.26384 (visited on 04/10/2024).

[26] Dwight Nishimura. *Principles of Magnetic Resonance Imaging*. English. Stanford Univ, Feb. 2010.

[27] Adam Paszke et al. "PyTorch: An Imperative Style, High-Performance Deep Learning Library". In: *Advances in Neural Information Processing Systems*. Vol. 32. Curran Associates, Inc., 2019. URL: https://proceedings.neurips.cc/paper/2019/hash/bdbca288fee7f92f2bfa9f7012727740-Abstract.html (visited on 04/10/2024).

[28] Fernando Pérez-García, Rachel Sparks, and Sébastien Ourselin. "TorchIO: A Python library for efficient loading, preprocessing, augmentation and patch-based sampling of medical images in deep learning". In: *Computer Methods and Programs in Biomedicine* 208 (Sept. 2021), p. 106236. ISSN: 0169-2607. DOI: 10.1016/j.cmpb.2021.106236. URL: https://www.sciencedirect.com/science/article/pii/S0169260721003102 (visited on 04/10/2024).

[29] Matthew E. Peters, Sebastian Ruder, and Noah A. Smith. "To Tune or Not to Tune? Adapting Pretrained Representations to Diverse Tasks". In: *Proceedings of the 4th Workshop on Representation Learning for NLP (RepL4NLP-2019)*. Ed. by Isabelle Augenstein et al. Florence, Italy: Association for Computational Linguistics, Aug. 2019, pp. 7–14. DOI: 10.18653/v1/W19-4302. URL: https://aclanthology.org/W19-4302 (visited on 04/10/2024).

[30] Jonas Pfeiffer et al. *Modular Deep Learning*. arXiv:2302.11529 [cs]. Jan. 2024. DOI: 10.48550/arXiv.2302.11529. URL: http://arxiv.org/abs/2302.11529 (visited on 04/10/2024).

[31] Donald B. Plewes and Walter Kucharczyk. "Physics of MRI: A primer". en. In: *Journal of Magnetic Resonance Imaging* 35.5 (2012). _eprint: https://onlinelibrary.wiley.com/doi/pdf/10.1002/jmri. pp. 1038–1054. ISSN: 1522-2586. DOI: 10.1002/jmri.23642. URL: https://onlinelibrary.wiley.com/doi/abs/10.1002/jmri.23642 (visited on 04/10/2024).

[32] Lutz Prechelt. "Early Stopping - But When?" en. In: *Neural Networks: Tricks of the Trade*. Ed. by Genevieve B. Orr and Klaus-Robert Müller. Berlin, Heidelberg: Springer, 1998, pp. 55–69. ISBN: 978-3-540-49430-0. DOI: 10.1007/3-540-49430-8_3. URL: https://doi.org/10.1007/3-540-49430-8_3 (visited on 04/10/2024).

[33] Kamisetty Ramam Rao and Patrick C. Yip. *The Transform and Data Compression Handbook*. en. Google-Books-ID: EgvOBQAAQBAJ. CRC Press, Oct. 2018. ISBN: 978-1-4200-3738-8.

[34] Olaf Ronneberger, Philipp Fischer, and Thomas Brox. "U-Net: Convolutional Networks for Biomedical Image Segmentation". en. In: *Medical Image Computing and Computer-Assisted Intervention – MICCAI 2015*. Ed. by Nassir Navab et al. Cham: Springer International Publishing, 2015, pp. 234–241. ISBN: 978-3-319-24574-4. DOI: 10.1007/978-3-319-24574-4_28.

[35] Sebastian Ruder. *An Overview of Multi-Task Learning in Deep Neural Networks*. arXiv:1706.05098 [cs, stat]. June 2017. DOI: 10.48550/arXiv.1706.05098. URL: http://arxiv.org/abs/1706.05098 (visited on 04/10/2024).

[36] Klaus Scheffler. "A pictorial description of steady-states in rapid magnetic resonance imaging". en. In: *Concepts in Magnetic Resonance* 11.5 (1999). _eprint: https://onlinelibrary.wiley.com/doi/pd 0534%281999%2911%3A5%3C291%3A%3AAID-CMR2%3E3.0.CO%3B2-J, pp. 291–304. ISSN: 1099-0534. DOI: 10.1002/(SICI)1099-0534(1999)11:5<291::AID-CMR2>3.0.CO;2-J. URL: https://onlinelibrary.wiley.com/doi/abs/10.1002/%28SICI%291099-0534%281999%2911%3A5%3C291%3A%3AAID-CMR2%3E3.0.CO%3B2-J (visited on 04/10/2024).

[37] Klaus Scheffler and Stefan Lehnhardt. "Principles and applications of balanced SSFP techniques". en. In: *European Radiology* 13.11 (Nov. 2003), pp. 2409–2418. ISSN: 1432-1084. DOI: 10.1007/s00330-003-1957-x. URL: https://doi.org/10.1007/s00330-003-1957-x (visited on 04/10/2024).

[38] Stephen M. Smith et al. "Advances in functional and structural MR image analysis and implementation as FSL". In: *NeuroImage*. Mathematics in Brain Imaging 23 (Jan. 2004), S208–S219. ISSN: 1053-8119. DOI: 10.1016/j.neuroimage.2004.07.051. URL: https://www.sciencedirect.com/science/article/pii/S1053811904003933 (visited on 04/10/2024).

[39] Jacques-Donald Tournier, Susumu Mori, and Alexander Leemans. "Diffusion Tensor Imaging and Beyond". In: *Magnetic Resonance in Medicine* 65.6 (June 2011), pp. 1532–1556. ISSN: 0740-3194. DOI: 10.1002/mrm.22924. URL: https://www.ncbi.nlm.nih.gov/pmc/articles/PMC3366862/ (visited on 04/10/2024).

[40] Tengfei Wang et al. *Pretraining is All You Need for Image-to-Image Translation*. arXiv:2205.12952 [cs]. May 2022. DOI: 10.48550/arXiv.2205.12952. URL: http://arxiv.org/abs/2205.12952 (visited on 04/10/2024).

[41] Zhou Wang et al. "Image quality assessment: from error visibility to structural similarity". In: *IEEE Transactions on Image Processing* 13.4 (Apr. 2004). Conference Name: IEEE Transactions on Image Processing, pp. 600–612. ISSN: 1941-0042. DOI: 10.1109/TIP.2003.819861. URL: https://ieeexplore.ieee.org/document/1284395 (visited on 04/10/2024).

[42] Matthias Weigel. "Extended phase graphs: Dephasing, RF pulses, and echoes - pure and simple". en. In: *Journal of Magnetic Resonance Imaging* 41.2 (2015). _eprint: https://onlinelibrary.wiley.c pp. 266–295. ISSN: 1522-2586. DOI: 10.1002/jmri.24619. URL: https://onlinelibrary.wiley.com/doi/abs/10.1002/jmri.24619 (visited on 04/10/2024).

[43] Qianye Yang et al. "MRI Cross-Modality Image-to-Image Translation". en. In: *Scientific Reports* 10.1 (Feb. 2020). Publisher: Nature Publishing Group, p. 3753. ISSN: 2045-2322. DOI: 10.1038/s41598-020-60520-6. URL: https://www.nature.com/articles/s41598-020-60520-6 (visited on 04/10/2024).

[44] Aston Zhang et al. *Dive into Deep Learning*. arXiv:2106.11342 [cs]. Aug. 2023. DOI: 10.48550/arXiv.2106.11342. URL: http://arxiv.org/abs/2106.11342 (visited on 04/10/2024).

[45] Richard Zhang et al. *The Unreasonable Effectiveness of Deep Features as a Perceptual Metric*. arXiv:1801.03924 [cs]. Apr. 2018. DOI: 10.48550/arXiv.1801.03924. URL: http://arxiv.org/abs/1801.03924 (visited on 04/10/2024).

Appendix

A. Supplementary Material

Figure .1. ***A. & B.*** *SNc and projections to the dorsal striatum in healthy subjects and patients with PD. In the healthy subject, the SNc is still highly pigmented due to the melanin-containing dopamine-producing cells being intact. The SNc projects to the striatum and delivers normal amounts of DA into the basal ganglia (BG) circuit. If the dopamine-producing neurons undergo apoptosis, the pigmentation decreases and so does the amount of dopamine adimnistered to the striatum.* ***C.*** *Photomicrographs of Lewy bodies.*